Exploring the difference in the mechanics of vascular smooth muscle cells from wild type and apolipoprotein-E knockout mice

Alex P. Rickel[1]*, Hanna J. Sanyour[1]*, Courtney Kinser[1], Nisha Khatiwada[1,2], Hayley Vogel[1], Zhongkui Hong[1,2]†

[1]Biomedical Engineering, University of South Dakota, 4800 N Career Avenue, Sioux Falls, SD, USA 57107

[2]Mechanical Engineering Department,Texas Tech University, 805 Boston Avenue, Lubbock, TX, USA 79409

*These two authors contributed equally

†To whom correspondence should be addressed:

Zhongkui Hong, Ph.D.,

Department of Mechanical Engineering

Texas Tech University

Box 4-1021

Lubbock, TX 79409-1021

Tel: (806)834-5395

Fax: (806)742-3540

E-mail : Zhongkui.Hong@ttu.edu

Running title: Vascular smooth muscle cell mechanics

Key words: Vascular smooth muscle cells, apolipoprotein-E knockout, atomic force microscopy, cell mechanics, cell adhesion, cell migration, cytoskeleton.

Supplemental Material available at

URL: https://figshare.com/s/91ca61cfca3dad64e7ac

DOI: https://doi.org/10.6084/m9.figshare.20682595

Abstract

Atherosclerosis-related cardiovascular diseases are a leading cause of mortality worldwide. Vascular smooth muscle cells (VSMCs) comprise the medial layer of the arterial wall and undergo phenotypic switching during atherosclerosis to a synthetic phenotype capable of proliferation and migration. The surrounding environment undergoes alterations in extracellular matrix (ECM) stiffness, composition, and increase in cholesterol content. Using an atherosclerotic murine model, we analyzed how the mechanics of VSMCs isolated from western diet fed apolipoprotein-E knockout ($ApoE^{-/-}$) and wild type (WT) mice were altered during atherosclerosis. Increased stiffness of $ApoE^{-/-}$ VSMCs correlated with a greater degree of stress fiber alignment as evidenced by atomic force microscopy (AFM)-generated force maps and stress fiber topography images. On type-1 collagen (COL1)-coated polyacrylamide (PA) gels (referred to as substrate) of varying stiffness, $ApoE^{-/-}$ VSMCs had lower adhesion forces to COL1 and N-Cadherin (N-Cad) compared to WT cells. $ApoE^{-/-}$ VSMC stiffness was significantly greater than WT cells. Cell stiffness increased with increasing substrate stiffness for both $ApoE^{-/-}$ and WT VSMCs . In addition, $ApoE^{-/-}$ VSMCs showed an enhanced

migration capability on COL1-coated substrates and a general decreasing trend in migration capacity with increasing substrate stiffness, correlating with lowered adhesion forces as compared to WT VSMCs. Altogether, these results demonstrate the potential contribution of the alteration in VSMC mechanics in the development of atherosclerosis.

Introduction

Despite strides of progress, cardiovascular disease has become the world's leading cause of mortality and atherosclerosis is a major contributor to this global epidemic (1). Atherosclerosis is a complex disease described as a chronic state of inflammation resulting in the formation of arterial plaques filled with lipid and cellular debris. Atherosclerotic plaque instability, fibrous cap thinning, and rupture cause a plethora of cardiovascular diseases such as heart attack, stroke, and peripheral vascular disease (2,3).

Vascular smooth muscle cells (VSMCs) are present in the medial layer of the vasculature providing arterial contraction and extracellular matrix (ECM) production to maintain optimal hemodynamic conditions (4). During the progression of atherosclerosis, VSMCs "respond to injury" and shift from a contractile to a synthetic phenotype to stabilize the plaque and form a fibrous cap. The VSMC phenotypic shift entails the reduction of contractile protein expression and the upregulation of cell proliferation, migration, and secretion of ECM proteins (5,6). VSMCs detach from neighboring cells and the surrounding ECM to migrate towards the intima during the development of atherosclerosis. Migrating VSMCs experience a wide range of microenvironments as the ECM within the plaque varies in composition and stiffness

(7). Type-1 collagen (COL1) was shown to be abundant near the stiffer fibrous cap but nearly absent within the softer, lipid rich necrotic core (8,9). In addition, migrating VSMCs actively modify ECM composition and stiffness through COL1 and fibronectin (FN) deposition (10,11).

Mechanotransduction at the cell-matrix interface plays a critical role in regulating cell adhesion to the ECM and cell migration (12-18). ECM stiffness has emerged as a prominent mechanical cue that precedes disease and drives its progression, by altering cellular behaviors such as phenotypic shifting (19) and aberrant cell migration in response to disease development (13,20). Cell-matrix mechanotransduction is regulated by factors including integrin expression and activity (21), and ECM composition (18); the latter has been demonstrated to be a critical determinant of cell behaviors (18,22,23). In our recent study, ECM proteins and substrate stiffness (where substrate refers to the material the cells were growing on) were found to synergistically regulate VSMC migration and cortical cytoskeleton organization (24). Moreover, VSMCs from apolipoprotein-E knockout ($ApoE^{-/-}$) mice were shown to constitute 30-70% of macrophage marker-positive (CD68) cells (25) and foam cells (26). In humans approximately 30-40% of CD68 positive cells and 50% of foam cells are of VSMC origin (25,27). VSMCs from $ApoE^{-/-}$ were shown to have altered structural and functional properties (28-31). Moreover, phenotypically altered VSMCs were shown to metabolize lipids differently to contractile VSMCs, partly due to the reduced cholesterol efflux mediated by ATP-binding cassette transporters and the decreased expression of cholesterol esterase, facilitating foam cell formation (27,32). Collectively, membrane

cholesterol and substrate stiffness were shown to coordinate and induce VSMC cytoskeleton remodeling and alteration of cell mechanics (33).

This study aims to investigate the difference in the mechanics of VSMCs isolated from ApoE$^{-/-}$ and wild type (WT) mice. Atomic force microscope (AFM) was employed to study N-cadherin (N-Cad) mediated cell-cell adhesion, integrin mediated cell-ECM adhesion forces, and stiffness of VSMCs cultured on elastically tunable substrates. AFM was also used to examine live VSMC submembranous cytoskeleton architecture. In addition, we inspected VSMCs migration dynamics and global cytoskeleton organization on elastically tunable COL1 coated substrates, mimicking the variation in environmental stiffness VSMCs experience in atherosclerosis. Our results demonstrated a significant difference in cell mechanics, cytoskeletal organization, and migratory behavior of VSMCs isolated from WT and ApoE$^{-/-}$ mice.

Materials and Methods

Mouse vascular smooth muscle isolation:

The mice used in this study were kept in accordance with the NIH guidelines (8th Edition of the Guide for the Care and Use of Laboratory Animals), and the animal use protocol was approved by the Laboratory Animal Use Committee of the University of South Dakota (#13-09-15-18C) and Sanford Institutional Care and Use Committee (#153-03-21C). For this study, male ApoE$^{-/-}$(B6.129P2-*Apoe*^{tm1Unc}/J, Jackson Laboratory) and male WT (C57BL/6J, Jackson Laboratory) mice were subjected to 10 weeks of western diet after reaching 8 weeks of age. To discern the influence of the western diet on cell mechanics, additional ApoE$^{-/-}$ and WT mice were fed normal chow for 18 weeks

for stiffness measurments on a plastic substrate only. Mice were euthanized using carbon dioxide (CO_2) asphyxiation and VSMCs were enzymatically isolated from the descending thoracic aorta and seeded onto 60 mm plastic dishes (Corning, Corning, NY). Cells were maintained in a DMEM-F12 (Invitrogen) medium supplemented with 10% fetal bovine serum (FBS, ATLANTA Biologicals, Lawrenceville, GA) in a humidified incubator with 5% CO2 at 37 °C (47) .

Elastically tunable ECM protein coated polyacrylamide gel preparation

Elastically tunable COL1 coated PA gels preparation was described in detail in our previous studies (24,33,34). Glass-bottom 50mm glass bottom dishes (MatTek, Ashland, MA, USA) or glass-bottom 6-well plates (Cellvis, Mountain View, CA, USA) were activated using 0.1N sodium hydroxide at 37 °C and grafted with one layer of (3-aminopropyl) triethoxysilane (APTS, Sigma, St. Louis, MO, USA). The aminated glass surface was then grafted with a 25 mm diameter PA gel using 0.5% glutaraldehyde (Sigma, St. Louis, MO, USA) as a crosslinker between the PA gel and aminated glass surface. The PA substrate was washed with 50 mM 4-(2-hydroxyethy)-1-peperazineethanesulfonic acid buffer (ThermoFisher Scientific, Waltham, MA, USA) to remove the unreacted monomer. The PA gel surface was coated with 300 µL of 1mM sulfosuccinimidyl 6-(4'-azido-2'-nitrophenylamion) hexanoate (sulfo-SANPAH, ThermoFisher Scientific, Waltham, MA, USA), activated for 10 min under UV light, and quickly washed with phosphate-buffered saline (PBS). This step was repeated to ensure sufficient coating of the crosslinker. After quick washes with PBS, one layer of COL1

(Sigma, St. Louis, MO, USA) (0.15mg/mL) was grafted to the PA surface. The different elasticities of the gels were previously determined using AFM indentation (34).

Cell migration studies

Cells were trypsinized, counted, and plated on elastically tunable COL1-coated PA gels at a density of 2500 cells/cm^2. Cells were allowed to attach to the plate in serum-free medium in a humidified incubator with 5% CO_2 at 37°C for 2 h. Afterwards, migration experiments were performed using a JuLI Stage Microscope (NanoEnTek Inc, South Korea). For each PA gel, five to ten regions of interest were chosen and imaged with a 10x objective every 10 min for 24 h. FIJI (FIJI is Just Image J, NIH, Bethesda, MD, USA) was used to analyze image stacks. Time-lapse image stacks were aligned using the plugin StackReg (Biomedical Imaging Group, Swiss Federal Institute of Technology Lausanne). Manual cell tracking was completed by tracing the position of the cell nucleus using the MtrackJ plugin. For each experiment, 90 cells were tracked from at least 3 replicates (24,35).

VSMC biomechanical characterization using AFM

VSMC stiffness, cell-cell, and cell-ECM adhesion were assessed in real time using an Asylum AFM System (Model MFP-3D-BIO, Asylum Research, Santa Barbara, CA) mounted on an inverted microscope (Model IX81, Olympus America Inc.). A 5 μm diameter glass microbead was glued to an AFM probe (MLCT-O10-D, Santa Barbara, CA; Bruker Corp.) and used for Young's modulus (E-modulus) measurement. Cell surface areas of 30 × 30 μm were automatically scanned and indented at 6×6 positions

with a 0.5 Hz indentation frequency and 1 μm/s approach/retraction velocity. A parabolic Hertz equation was used to estimate VSMC stiffness (34,36). For adhesion force measurement, cell surfaces were probed at a 0.05 Hz indentation frequency and 0.1 μm/s approach/retraction velocity using an AFM probe (MLCT, Santa Barbara, CA; Bruker Corp.) functionalized with N-cadherin (Human N-Cad R&D Systems, Minneapolis, MN) (10μg/ml) or COL1 (1mg/ml). The AFM force curves were analyzed using a proprietary MATLAB program (R2016a, Mathworks). The product of the AFM probe spring constant and the height of ruptures (adhesion events) on a retraction force curve were identified and used to compute adhesion forces. The total average adhesion force is the product of average adhesion force and number of ruptures. Adhesion and stiffness testing of VSMCs cultured on elastically tunable PA gels were limited to measuring a single position. Primary VSMCs attached to at least two other cells were selected and indented at a site between the cell edge and nucleus. The thermal noise amplitude method was used to calibrate each AFM probe after each adhesion measurement and before each stiffness measurement experiment (37,38).

Live VSMC cytoskeletal imaging using AFM and image processing

Contact mode AFM imaging was employed to assess VSMC cytoskeleton architecture in real time. Using an AFM stylus probe (model MLCT-C, k = 15 pN/nm, Bruker, Santa Barbara, CA, USA), a 30 × 30 μm cell surface area was imaged with the digital density of 512 × 512 pixels. The scanning frequency was 0.3 Hz. The obtained height and deflection images were analyzed using a proprietary MATLAB program to analyze cell fiber orientation and density as described in our previous work (24,33,35). Stress fiber

area fraction is defined as the ratio of the whole cell surface area compared to that covered by stress fibers. The area fraction was computed from AFM height images post flattening and background noise elimination to improve the contrast between the background (non-stress fiber area) and the foreground (stress fibers). AFM deflection images were utilized to determine cytoskeletal stress fiber orientation. Finally, cell surface roughness was determined from height images using the built-in function of the AFM Asylum Research software.

Confocal imaging and image processing

VSMCs were passaged and seeded onto COL1-coated PA gels at a density of 10,000 cells/cm^2. Cells were fixed at 60-80% confluency with 4% paraformaldehyde in phosphate-buffered saline (PBS) (Affymetrix, CA) for 20 min at room temperature followed by several rinses with PBS. VSMCs were permeabilized with 0.1% Triton X-100 in PBS for 5 min and rinsed with PBS. F-actin cytoskeleton was stained with a 1:1000 dilution of phalloidin (Phalloidin-iFluor 488, Abcam, Cambridge, U.K.) in 1% bovine serum albumin/PBS for 20 min and rinsed with PBS. The nuclei were counterstained with a 1:1000 dilution of Hoechst 33342 (BD Biosciences, San Jose, CA) dissolved in PBS for 10 min followed by a final rinse with PBS. VSMCs were imaged using a laser scanning confocal microscope (Olympus IX83 FV1200, Olympus Life Science) at a 1024 × 1024-pixel resolution and z-height of 0.38 μm. Z-stacks were flattened and manually segmented by tracing VSMCs in contact with at least one other cell. As previously described, a series of elongated Laplacian-of- Gaussian (eLoG)

filters were used to convolve flattened z-stacks to detect total cellular cytoskeletal fiber orientation (24,39).

Statistical testing

One-way ANOVA with Tukey's post hoc test was used to infer statistical significance for all experiments. A value of *P ≤ 0.05, **P ≤ 0.01, and ***P ≤ 0.001 was considered statistically significant. All data were reported as the mean ± standard error of the mean (SEM).

Results

WT and ApoE$^{-/-}$ VSMC stiffness and submembranous stress fiber orientation measurement using AFM

Using a 5μm diameter glass microbead glued to an AFM probe, 30 × 30μm cell surface areas were automatically scanned and indented at 6×6 positions (Fig. 1A). Normal diet fed ApoE$^{-/-}$ and WT mice had no significant difference in cell stiffness (Fig. 1B). Stiffness maps for WT and ApoE$^{-/-}$ VSMCs are presented in Figure 1 C and D, respectively, with ApoE$^{-/-}$ VSMCs cultured on a plastic plate significantly stiffer than WT VSMCs (Fig. 1E).

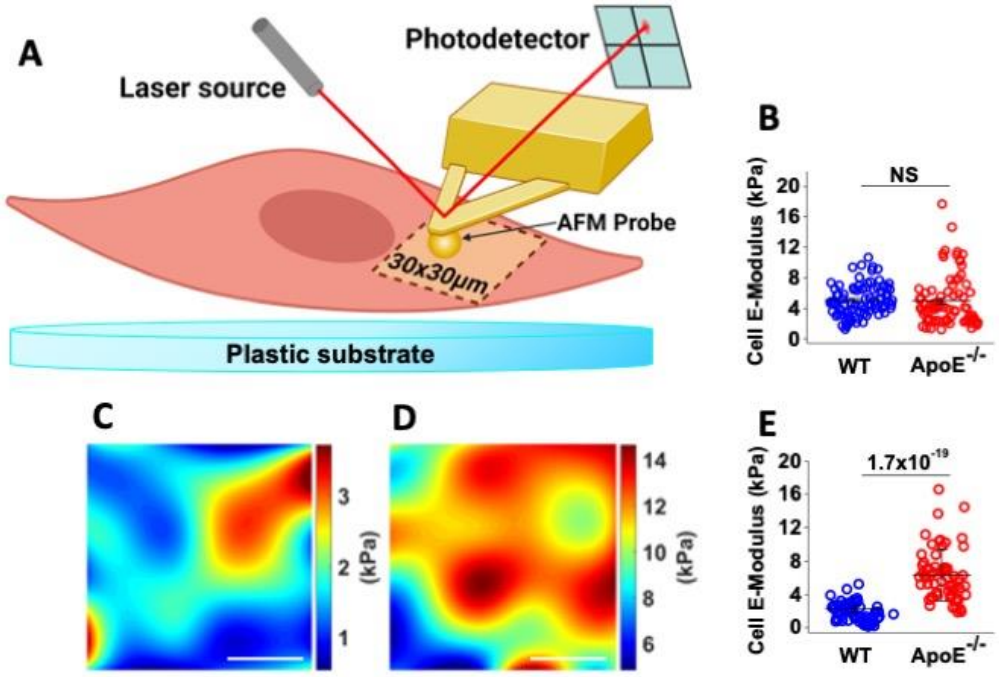

Fig. 1. Live WT and ApoE$^{-/-}$ VSMC stiffness maps. (A) 30 × 30 μm cell surface areas were automatically scanned and indented at 6×6 positions with a glass bead. **(B)** Average stiffness for normal diet fed ApoE$^{-/-}$ and WT VSMCs. **(C, D)** Stiffness force maps for WT and ApoE$^{-/-}$ VSMCs, respectively. **(E)** Average stiffness for western diet fed WT and ApoE$^{-/-}$ VSMCs. No significant difference in E-modulus was observed between ApoE$^{-/-}$ and WT VSMCs. Western diet fed ApoE$^{-/-}$ VSMCs had a significantly higher E-modulus compared to WT VSMCs. All data are presented as the mean ± SEM. (n ≥ 60 cells across six different mice). Scale bar in lower right corner represents 10 μm.

Submembranous stress fiber topography was acquired by scanning a 30 × 30 μm area in contact mode (Fig. 2A). Figure 2B and 2C are representative three-dimensional 30 × 30 μm cell surface area stress fiber topography of a WT and ApoE$^{-/-}$ VSMC, respectively. The stress fiber area fraction was unchanged for both cell types

suggesting similar stress fiber area coverage within the cell body (Fig. 2D). The normalized percentage circular histograms along the dominant orientation (Fig. 2E and F) demonstrates a clear difference in stress fiber orientation between WT and ApoE$^{-/-}$ VSMCs. For WT and ApoE$^{-/-}$ VSMCs, Figure 2G illustrates the percent frequency of average stress fiber orientation, normalized along the dominant angle, fitted with a first order Gaussian function. The summarized percent frequency of stress fibers oriented around the dominant angle (±20°) indicates that ApoE$^{-/-}$ VSMCs have significantly greater stress fiber alignment as compared to the WT (Fig. 2H). The surface roughness average (the absolute difference in the peak and valley value of measured microscopic surface peaks and valleys of VSMC topographical images) of ApoE$^{-/-}$ VSMCs was significantly greater than WT VSMCs (Fig. 2I).

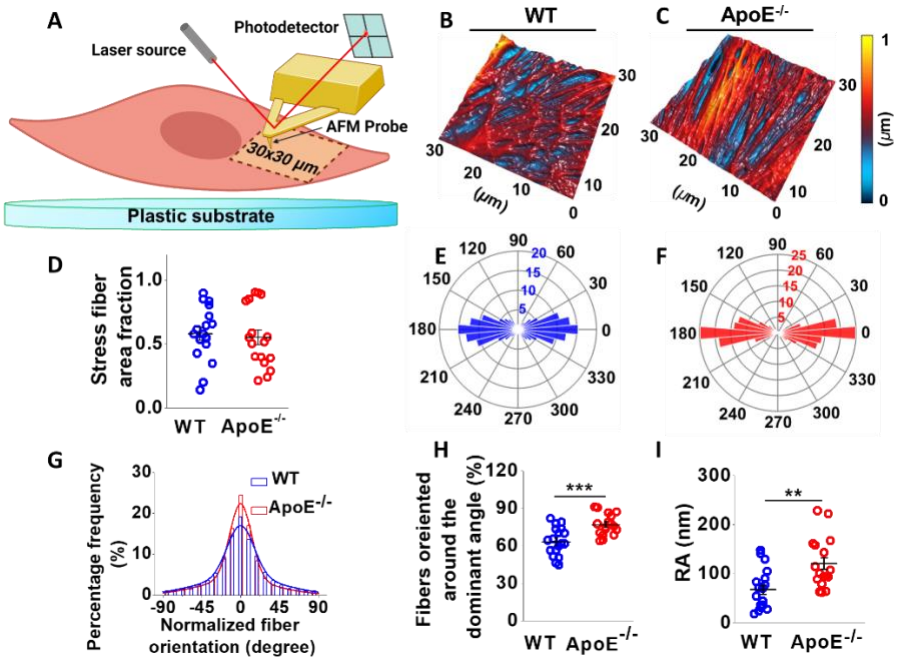

Fig. 2. Live WT and ApoE$^{-/-}$ VSMC submembranous stress fibers orientation measurement. (A) 30 × 30μm areas were scanned for overall VSMCs stiffness measurement. **(B**, **C)** Representative 30 × 30 μm three-dimensional stress fiber

topography of a WT and ApoE$^{-/-}$ VSMCs used for live VSMCs stress fiber orientation and area fraction analysis. (**D)** Average area fraction of VSMC submembranous actin stress fibers. **(E, F)** Circular histogram, showing the normalized stress fiber orientation of WT and ApoE$^{-/-}$ deflection images, respectively. **(G)** The average stress fiber orientation percentage histogram for WT and ApoE$^{-/-}$ VSMCs, in which the dominant stress fiber orientation angle was set as zero degrees for each cell**. (H)** The summarized percentage frequency of dominant fiber orientation (−20°∼+20°) **(I)** Average stress fiber surface roughness average. ApoE$^{-/-}$ VSMCs have significantly greater stress fiber alignment surface roughness compared to WT VSMCs. All data are presented as the mean ± SEM (n= 16 cells across six different mice).

Stiffness, cell-cell adhesion, and cell-ECM adhesion of WT and ApoE$^{-/-}$ VSMCs on COL1-coated gel substrates.

WT and ApoE$^{-/-}$ VSMCs were cultured on elastically tunable COL1-coated gels and probed with the AFM to measure stiffness (Fig 3A). The stiffness of these substrates was previously measured with AFM and determined to be 28 and 103 kPa (34). ApoE$^{-/-}$ VSMCs cultured on 28 and 103 kPa substrates had a significantly higher E-modulus compared to WT and those cultured on the stiffer substrate had a higher E-modulus for both ApoE$^{-/-}$ and WT VSMCs (Fig. 3B).

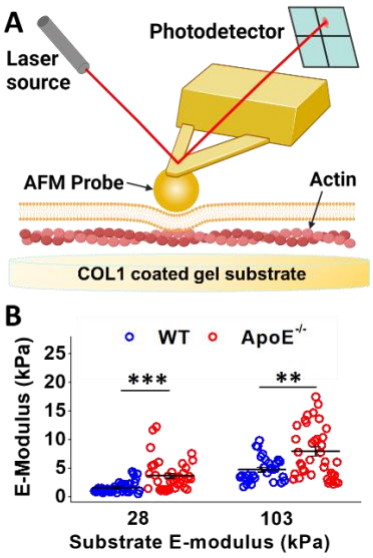

Fig. 3. Measuring stiffness of WT and ApoE$^{-/-}$ VSMCs on COL1-coated gel substrates. (A) WT or ApoE$^{-/-}$ VSMCs were cultured on elastically tunable COL1-coated PA gels and indented with a glass bead at a single point. **(B)** Average VSMCs E-modulus of VSMCs on 28 and 103 kPa substrates. ApoE$^{-/-}$ VSMCs cultured on 28 and 103 kPa substrates had a significantly higher E-modulus compared to WT VSMCs and demonstrated increased E-modulus when cultured on stiffer substrates. All data are presented as the mean ± SEM. (n ≥ 60 cells across six different mice for each group)

Cell- ECM and cell-cell adhesion were investigated with a COL1 or N-Cad coated stylus probes (Fig. 4A). Cell-ECM average adhesion force of ApoE$^{-/-}$ VSMCs on the 28 and 103 kPa substrates was significantly lower compared to WT, with both WT and ApoE$^{-/-}$ VSMCs exhibiting slightly reduced adhesion force on the 103 kPa substrate (Fig. 4B). Cell-cell adhesion was measured using an AFM stylus probe coated with N-Cad (Fig 4A). ApoE$^{-/-}$ VSMCs had a significantly lower adhesion force to N-Cad compared to WT on the 28 and 103 kPa substrates. The average adhesion force increased slightly

with increased substrate stiffness for both WT and ApoE$^{-/-}$ VSMCs (Fig. 4C). Cell counting of VSMC nuclei showed a slight decreasing trend in the adhesion rate of ApoE$^{-/-}$ compared to WT VSMCs after allowing to attach to substrate for 30 min (Fig. S1). However, the diference was not statistically significant ($p>0.05$).

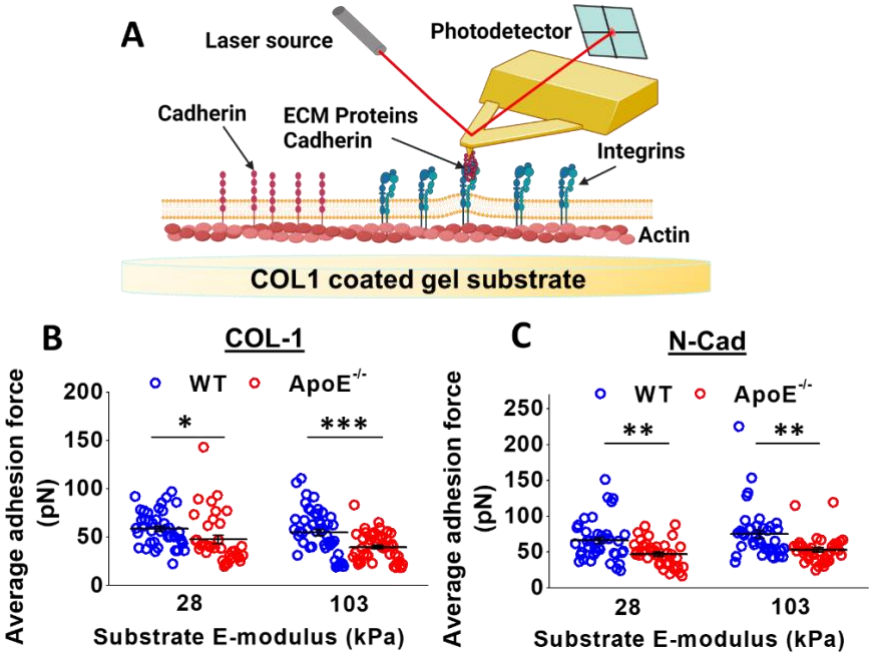

Fig. 4. Measuring cell-ECMI adhesion and cell-cell adhesion of WT and ApoE$^{-/-}$ VSMC on COL1-coated gel substrates. (A) AFM tips were coated with ECM proteins or cadherin and used to measure adhesion forces. **(B)** Total average adhesion force to cell-ECM adhesion protein COL1. **(C)** Average adhesion force to N-cadherin**.** ApoE$^{-/-}$ VSMCs demonstrated a significantly lower adhesion force to COL1 and N-Cad compared to WT cells. All data are presented as the mean ± SEM. (n ≥60 cells across six different mice for each group)

WT and ApoE$^{-/-}$ VSMCs migration dynamics on COL1-coated gel substrates.

WT and ApoE$^{-/-}$ VSMC migration were measured on 28 and 103 kPa COL1-coated PA gels (Fig. 5A). The average migration distance over time was significantly greater for ApoE$^{-/-}$ VSMCs compared to WT on both 28 and 103 kPa substrates (Fig. 5B and C). However, substrate stiffness did not have a statistically significant effect on migration for both WT and ApoE$^{-/-}$ VSMCs (Fig. 5D).

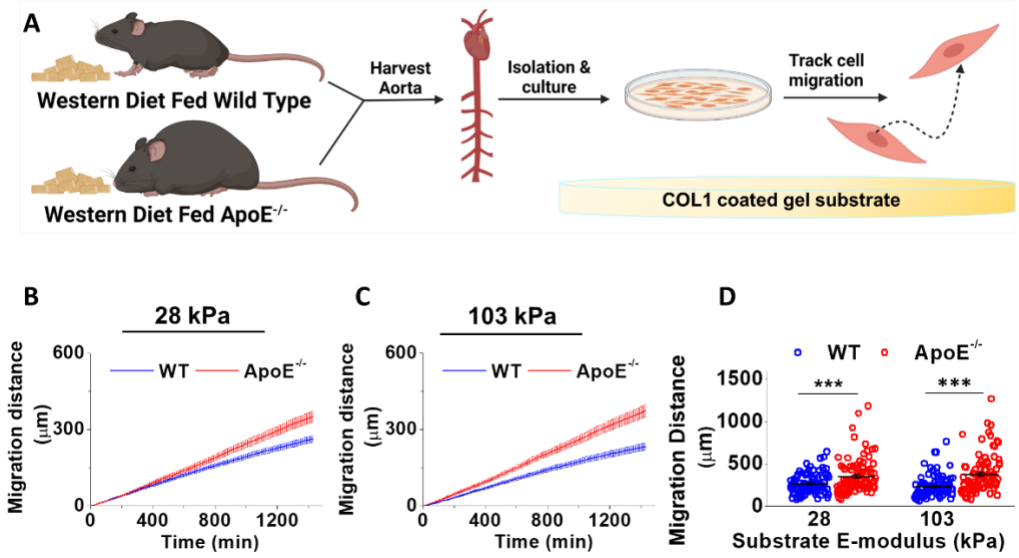

Fig. 5. WT and ApoE$^{-/-}$ VSMCs migration dynamics on COL1-coated gel substrates. (A) VSMCs isolated from WT and ApoE$^{-/-}$ mice were seeded onto COL1-coated PA gels to track cell migration. **(B, C)** Average distance vs time for WT and ApoE$^{-/-}$ VSMCs the 28 and 103 kPa COL1-coated substrates, respectively. **(D)** Migration distance of VSMCs on different substrate stiffnesses. ApoE$^{-/-}$ VSMCs demonstrated a higher migration capacity compared to WT cells. All data are presented as the mean ± SEM (n = 90 cells across three different mice for each group).

WT and ApoE$^{-/-}$ VSMC global cytoskeleton architecture

Global cytoskeletal architecture was characterized using confocal microscopy through the study of stress fiber orientation in WT and ApoE$^{-/-}$ VSMCs on 28 and 103 kPa COL1-coated gels substrate. Fluorescent actin cytoskeleton z-stack images, represented in Figure 6 for WT and ApoE$^{-/-}$ VSMCs for 28 kPa and 103 kPa COL1 substrates (Fig. 6A, B, C, and D, respectively), were used to generate the corresponding segmented stress fiber orientation color maps (Fig. 6E, F, G, and H) using a proprietary MATLAB program. On both 28 and 103 kPa COL1-coated substrates, ApoE$^{-/-}$ VSMCs exhibited a high degree of intracellular color map uniformity indicating close alignment of actin filaments, while more varied coloration within WT VSMCs indicates greater dispersion of actin filaments (Fig. 6E, F, G, and H). This observation was consistent with qualitative analysis of F-actin orientation, as illustrated by circular histograms with a tighter grouping around the dominant orientation angle for ApoE$^{-/-}$ VSMCs on both substrates compared to WT VSMCs, especially on the 103 kPa substrate (Fig. 6I, J, K, and L). Normalized fiber orientation histograms confirmed increased frequency of fiber orientation about the dominant angle for ApoE$^{-/-}$ VSMCs compared to WT, with a slightly higher peak on the 28 kPa substrate and a more pronounced peak on the 103 kPa substrate (Fig. 6M and O). ApoE$^{-/-}$ VSMC global stress fiber alignment around the dominant orientation angle was significantly greater than WT on the 103 kPa substrate, with the ApoE$^{-/-}$ VSMCs showing a more orientated structure and the WT a more dispersed structure (Fig. 6P). No significant difference in stress fiber orientation was seen on the 28 kPa substrate, though ApoE$^{-/-}$ orientation had a slightly higher average (Fig. 6N).

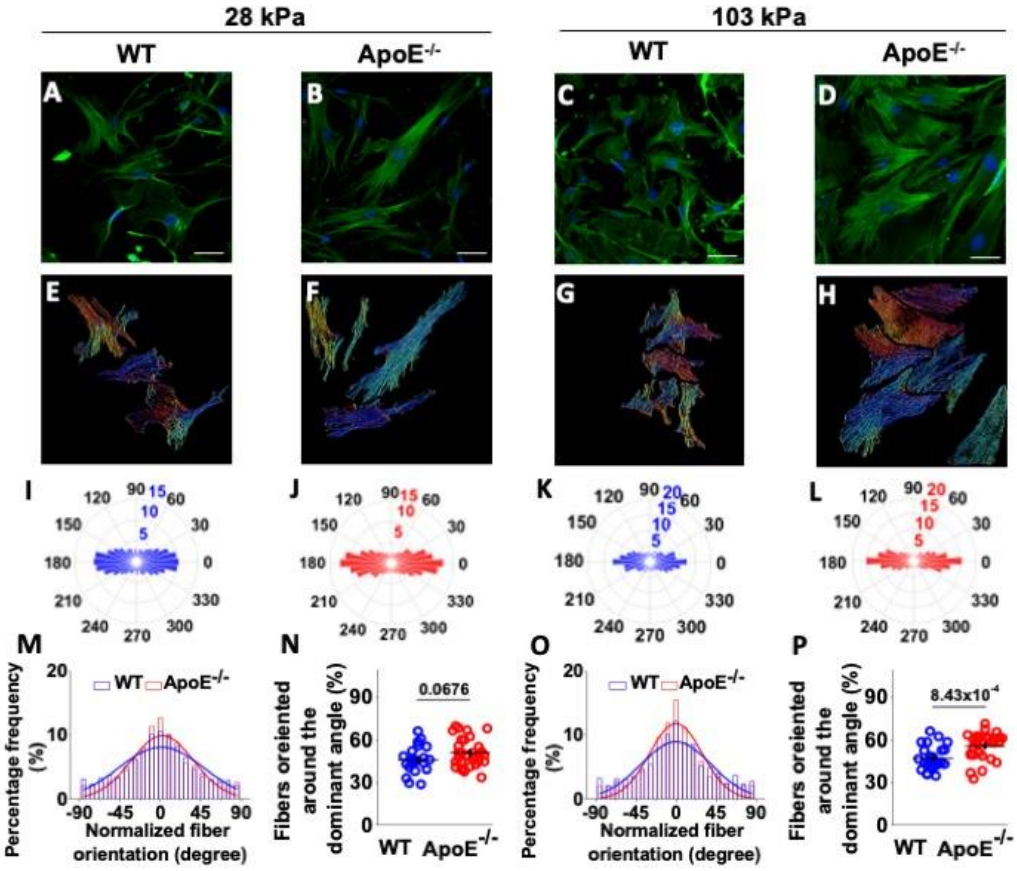

Fig. 6. Confocal imaging of WT and ApoE$^{-/-}$ VSMC cytoskeleton orientation. (A, B, C, D) Representative fluorescent z-stack images of the actin cytoskeleton for WT and ApoE$^{-/-}$ VSMCs on the 28 and 103 kPa COL1-coated substrates. **(E, F, G, H)** The corresponding segmented color maps showing cytoskeleton orientation computed from the confocal images. **(I, J, K, L)** Corresponding circular histograms showing the normalized F-actin fiber orientation. **(M, O)** Average normalized fiber orientation where the dominant angle is set as zero degrees on the 28 and 103 kPa substrate, respectively. **(N, P)** Summarized percentage frequency of fibers orientated around the dominant angle. ApoE$^{-/-}$ VSMCs on the 103 kPa substrate demonstrated a greater cytoskeletal alignment compared to WT cells. All data are presented as the mean ±

SEM (n > 60 cells from at least 25 images across three different mice for each group). Scale bars in lower right corner represent 50 μm.

Discussion

We have previously demonstrated the effects of cholesterol and substrate stiffness on VSMC biomechanics including changes in cytoskeletal organization, cellular stiffness, adhesion forces, migration, and vasoactivity through *in vitro* manipulation of cholesterol using methyl-β-cyclodextrin and statins in rat VSMCs (24,33,35). We sought to expand these studies and utilize a murine atherosclerosis model. ApoE$^{-/-}$ mice exhibit hypercholesterolemia and spontaneous development of atherosclerosis with a Western diet (40). Hypercholesterolemia from the Western diet significantly altered VSMC biomechanics as normal diet ApoE$^{-/-}$ and WT VSMCs had no significant difference in elastic modulus whereas VSMCs isolated from ApoE$^{-/-}$ mice fed a Western diet exhibited a higher elastic modulus compared to WT, an effect that was also seen with increased substrate stiffness (33). ApoE$^{-/-}$ VSCMs had a more aligned arrangement of cortical actin as well as lowered adhesion for both N-Cad and COL1 compared to WT. In addition, ApoE$^{-/-}$ VSMCs migrated further than the WT on both 28 kPa and 103 kPa substrates and exhibited greater cytoskeletal alignment, particularly on the stiffer substrate.

These results largely corroborate our previously reported results, providing further insight into VSMC behavior during the progression of atherosclerosis. ApoE$^{-/-}$ VSMCs were stiffer than WT VSMCs which is consistent with the enhanced alignment of cytoskeletal stress fiber orientation. The cytoskeleton has been shown to be a major

contributor to cell stiffness; and actin disruption resulted in decreased stiffness (41). Furthermore, several studies in erythrocytes have shown that increased cholesterol promotes tighter membrane cytoskeleton linkage and increased resistance to cell lysis (42-44). Other studies have implicated ezrin, radixin, and moesin (ERM), which link the membrane to the actin cytoskeleton, to influence cytoskeletal architecture and stiffness, though their exact function has yet to elucidated in VSMCs as ERM function appears to differ between cell types (45). However, cholesterol has been shown to regulate ERM proteins. During adipogenic differentiation, cholesterol enrichment upregulated phosphorylated moesin and downregulated phosphorylated ezrin, decreasing stiffness, while cholesterol depletion had the opposite affect (46). We assessed total ERM, total phospho-ERM, ezrin, moesin, myosin light chain 2, and myosin light chain kinase (MLCK) expression by immunoblotting and found no significant difference in expression between ApoE$^{-/-}$ and WT VSMCs (Fig. S2). However, some interesting trends were observed, particularly for ezrin and MLCK that are worth further investigation, particularly with non-passaged cells (Fig. S2A.). In addition, the cytoskeleton is connected to the ECM through focal adhesions that physically couple cells to the matrix (47). In our previous work, we showed that both membrane cholesterol and substrate stiffness co-ordinate to induce the remodeling of the cytoskeleton and alter VSMC integrin mediated biomechanics (33). Thus, increased VSMC stiffness with increased substrate stiffness could be attributed in part to enhanced transduction of tension from substrates to the cell surface and VSMC cholesterol content.

ApoE$^{-/-}$ VSMCs had a significantly greater migration distance compared to WT VSMCs on each of the different substrate stiffnesses. This behavior aligns with VSMCs

394 demonstrating enhanced proliferation and migration with the progression of
395 atherosclerosis following the switch from a contractile to synthetic phenotype. Enhanced
396 cell migration distance is likely the result of a combination of changing adhesion forces
397 and cytoskeleton dynamics. Increased plasma membrane cholesterol content has been
398 associated with reduction in maximum protrusion force and subsequent increase in
399 protrusion length in human embryonic kidney cells during optical tweezer manipulation
400 (41). As the formation of filopodia and lamellipodia drives cell migration, the ability to
401 easily form longer protrusions could partially explain ApoE$^{-/-}$ VSMC behavior. Ezrin has
402 also been demonstrated to influence migration and cytoskeleton stiffness with
403 constitutively activated ezrin resulting in greater migration and cytoskeleton stiffness
404 (48). Adhesion to the ECM through focal adhesion complexes is another critical
405 component to cell migration. A significant reduction in adhesion forces to N-Cad and
406 COL1 was observed in ApoE$^{-/-}$ VSMCs for each substrate stiffness compared to WT
407 VSMCs. Although not significant, we observed an increase in cell adhesion force to N-
408 Cad with increased substrate stiffness in both ApoE$^{-/-}$ and WT VSMC. ApoE$^{-/-}$ VSMCs
409 exhibited reduced N-Cad adhesion force and greater migration compared to WT
410 VSMCs, consistent with chemotaxis migration assays that suggest N-Cad has an anti-
411 migratory effect and that downregulation of N-Cad promotes cell migration (49,50).
412 Alternatively, ApoE$^{-/-}$ VSMCs exhibited lower COL1 adhesion force and increased
413 migration compared to WT VSMCs. With increased substrate stiffness from 28 kPa to
414 103 kPa, ApoE$^{-/-}$ VSMC migration increased while COL1 adhesion was reduced.
415 Bangasser *et al*. proposed a cell migration model wherein substrate stiffness modulates

cell migration dependent upon the number of motors and clutches, for which an optimal range promotes fast migration by nonlinear trends (20).

Conclusion

In summary, hypercholesterolemia from the Western diet likely had a significant causal effect on the observed difference in cell biomechanics. ApoE$^{-/-}$ VSMCs had a higher stiffness compared to WT VSMCs as a result of greater cytoskeleton stress fiber alignment. Increasing substrate stiffness had a synergistic affect, increasing cell stiffness for both WT and ApoE$^{-/-}$ VSMCs, though to a greater degree for ApoE$^{-/-}$ VSMCs, and increasing cytoskeleton stress fiber alignment in ApoE$^{-/-}$ VSMCs. Adhesion forces to N-Cad and COL1 were lower for ApoE$^{-/-}$ VSMCs compared to WT, associated with the increased migration of ApoE$^{-/-}$ VSMCs compared to WT VSMCs. These results support our hypothesis that atherosclerosis alters the mechanical properties of VSMCs and provide insight into underlying mechanisms that may lead to future novel therapeutic approaches.

Author contributions

A.R. conducted cell isolation and culture, cell migration study, confocal imaging, western blotting, cell counting assay, data analysis, and wrote the manuscript. H.S. conducated cell isolation and culture, AFM biomechanical testing and imaging, data analysis, and wrote the manuscript. C.K. conducted cell isolation and culture, confocal imaging, data analysis, and edited the manuscript. N.K. performed western blots and

editted the manuscript. H.V. performed cell count assay and editted the manuscript. Z.H. designed the study, analyzed data, and wrote the manuscript.

Acknowledgements

This work was supported, in part, by the National Science Foundation 2127031 (to Z. H.) and the National Institutes of Health R15HL147214 (to Z. H.). Panel (A)s for Figures 1–5 were created using Biorender.com.

Declaration of Interests

The authors declare that they have no competing interests.

References

1. Roth, G., G. Mensah, C. Johnson, G. Addolorato, E. Ammirati, L. Baddour, N. Barengo, A. Beaton, E. Benjamin, C. Benziger, A. Bonny, M. Brauer, M. Brodmann, T. Cahill, J. Carapetis, A. Catapano, S. Chugh, L. Cooper, J. Coresh, M. Criqui, N. DeCleene, K. Eagle, S. Emmons-Bell, V. Feigin, J. Fernández-Solà, G. Fowkes, E. Gakidou, S. Grundy, F. He, G. Howard, F. Hu, L. Inker, G. Karthikeyan, N. Kassebaum, W. Koroshetz, C. Lavie, D. Lloyd-Jones, H. Lu, A. Mirijello, A. Temesgen, A. Mokdad, A. Moran, P. Muntner, J. Narula, B. Neal, M. Ntsekhe, G. Moraes de Oliveira, C. Otto, M. Owolabi, M. Pratt, S. Rajagopalan, M. Reitsma, A. Ribeiro, N. Rigotti, A. Rodgers, C. Sable, S. Shakil, K. Sliwa-Hahnle, B. Stark, J. Sundström, P. Timpel, I. Tleyjeh, M. Valgimigli, T. Vos, P. Whelton, M. Yacoub, L. Zuhlke, C. Murray, V. Fuster, and G. B. o. C. D. W. G. GBD-NHLBI-JACC. 2020. Global Burden of Cardiovascular Diseases and Risk Factors, 1990-2019: Update From the GBD 2019 Study. *J Am Coll Cardiol*. 76(25):2982-3021.

2. Kobiyama, K., and K. Ley. 2018. Atherosclerosis. *Circ Res*. 123(10):1118-1120.
3. Wolf, D., and K. Ley. 2019. Immunity and Inflammation in Atherosclerosis. *Circ Res*. 124(2):315-327.
4. Lacolley, P., V. Regnault, A. Nicoletti, Z. Li, and J. Michel. 2012. The vascular smooth muscle cell in arterial pathology: a cell that can take on multiple roles. *Cardiovasc Res*. 95(2):194-204.
5. Basatemur, G., H. Jørgensen, M. Clarke, M. Bennett, and Z. Mallat. 2019. Vascular smooth muscle cells in atherosclerosis. *Nat Rev Cardiol*. 16(12):727-744.
6. Bennett, M. R., S. Sinha, and G. K. Owens. 2016. Vascular Smooth Muscle Cells in Atherosclerosis. *Circ Res*. 118(4):692-702.
7. Johnson, J. 2014. Emerging regulators of vascular smooth muscle cell function in the development and progression of atherosclerosis. *Cardiovasc Res*. 103(4):452-460.
8. Raines, E. W. 2000. The extracellular matrix can regulate vascular cell migration, proliferation, and survival: relationships to vascular disease. *Int J Exp Pathol*. 81(3):173-182.
9. Tracqui, P., A. Broisat, J. Toczek, N. Mesnier, J. Ohayon, and L. Riou. 2011. Mapping elasticity moduli of atherosclerotic plaque in situ via atomic force microscopy. *J Struct Biol*. 174(1):115-123.
10. Rocnik, E. F., B. M. Chan, and J. G. Pickering. 1998. Evidence for a role of collagen synthesis in arterial smooth muscle cell migration. *J Clin Invest*. 101(9):1889-1898.
11. van Helvert, S., and P. Friedl. 2016. Strain Stiffening of Fibrillar Collagen during Individual and Collective Cell Migration Identified by AFM Nanoindentation. *ACS Appl Mater Interfaces*. 8(34):21946-21955.
12. Canver, A., O. Ngo, R. Urbano, and A. Clyne. 2016. Endothelial directed collective migration depends on substrate stiffness via localized myosin contractility and cell-matrix interactions. *J Biomech*. 49(8):1369-1380.

13. Hadden, W., J. Young, A. Holle, M. McFetridge, D. Kim, P. Wijesinghe, H. Taylor-Weiner, J. Wen, A. Lee, K. Bieback, B. Vo, D. Sampson, B. Kennedy, J. Spatz, A. Engler, and Y. Choi. 2017. Stem cell migration and mechanotransduction on linear stiffness gradient hydrogels. *Proc Natl Acad Sci U S A*. 114(22):5647-5652.
14. Li, S., J. Guan, and S. Chien. 2005. Biochemistry and biomechanics of cell motility. *Annu Rev Biomed Eng*. 7:105-150.
15. Lu, X., Z. Ding, F. Xu, Q. Lu, and D. L. Kaplan. 2019. Subtle Regulation of Scaffold Stiffness for the Optimized Control of Cell Behavior. *ACS Applied Bio Materials*. 2(7):3108-3119.
16. Nalluri, S., J. O'Connor, and E. Gomez. 2015. Cytoskeletal signaling in TGFβ-induced epithelial-mesenchymal transition. *Cytoskeleton (Hoboken)*. 72(11):557-569.
17. Saavedra, J., I. Armando, C. Bregonzio, A. Juorio, M. Macova, J. Pavel, and E. Sanchez-Lemus. 2006. A centrally acting, anxiolytic angiotensin II AT1 receptor antagonist prevents the isolation stress-induced decrease in cortical CRF1 receptor and benzodiazepine binding. *Neuropsychopharmacology*. 31(6):1123-1134.
18. Hartman, C., B. Isenberg, S. Chua, and J. Wong. 2016. Vascular smooth muscle cell durotaxis depends on extracellular matrix composition. *Proc Natl Acad Sci U S A*. 113(40):11190-11195.
19. Gomez, E., Q. Chen, N. Gjorevski, and C. Nelson. 2010. Tissue geometry patterns epithelial-mesenchymal transition via intercellular mechanotransduction. *J Cell Biochem*. 110(1):44-51.
20. Bangasser, B. L., G. A. Shamsan, C. E. Chan, K. N. Opoku, E. Tuzel, B. W. Schlichtmann, J. A. Kasim, B. J. Fuller, B. R. McCullough, S. S. Rosenfeld, and D. J. Odde. 2017. Shifting the optimal stiffness for cell migration. *Nat Commun*. 8:15313.
21. Wang, X., J. Sun, Q. Xu, F. Chowdhury, M. Roein-Peikar, Y. Wang, and T. Ha. 2015. Integrin Molecular Tension within Motile Focal Adhesions. *Biophys J*. 109(11):2259-2267.

22. Seong, J., A. Tajik, J. Sun, J. Guan, M. Humphries, S. Craig, A. Shekaran, A. García, S. Lu, M. Lin, N. Wang, and Y. Wang. 2013. Distinct biophysical mechanisms of focal adhesion kinase mechanoactivation by different extracellular matrix proteins. *Proc Natl Acad Sci U S A*. 110(48):19372-19377.
23. Thakar, R., F. Ho, N. Huang, D. Liepmann, and S. Li. 2003. Regulation of vascular smooth muscle cells by micropatterning. *Biochem Biophys Res Commun*. 307(4):883-890.
24. Rickel, A. P., H. J. Sanyour, N. A. Leyda, and Z. Hong. 2020. Extracellular Matrix Proteins and Substrate Stiffness Synergistically Regulate Vascular Smooth Muscle Cell Migration and Cortical Cytoskeleton Organization. *ACS Applied Bio Materials*. 3(4):2360-2369.
25. Shankman, L., D. Gomez, O. Cherepanova, M. Salmon, G. Alencar, R. Haskins, P. Swiatlowska, A. Newman, E. Greene, A. Straub, B. Isakson, G. Randolph, and G. Owens. 2015. KLF4-dependent phenotypic modulation of smooth muscle cells has a key role in atherosclerotic plaque pathogenesis. *Nat Med*. 21(6):628-637.
26. Wang, Y., J. Dubland, S. Allahverdian, E. Asonye, B. Sahin, J. Jaw, D. Sin, M. Seidman, N. Leeper, and G. Francis. 2019. Smooth Muscle Cells Contribute the Majority of Foam Cells in ApoE (Apolipoprotein E)-Deficient Mouse Atherosclerosis. *Arterioscler Thromb Vasc Biol*. 39(5):876-887.
27. Allahverdian, S., A. C. Chehroudi, B. M. McManus, T. Abraham, and G. A. Francis. 2014. Contribution of intimal smooth muscle cells to cholesterol accumulation and macrophage-like cells in human atherosclerosis. *Circulation*. 129(15):1551-1559.
28. Ali, K., S. Lund-Katz, J. Lawson, M. Phillips, and D. Rader. 2008. Structure-function properties of the apoE-dependent COX-2 pathway in vascular smooth muscle cells. *Atherosclerosis*. 196(1):201-209.
29. Ewart, M., S. Kennedy, D. Macmillan, A. Raja, I. Watt, and S. Currie. 2014. Altered vascular smooth muscle function in the ApoE knockout mouse during the progression of atherosclerosis. *Atherosclerosis*. 234(1):154-161.

30. Ishigami, M., D. Swertfeger, M. Hui, N. Granholm, and D. Hui. 2000. Apolipoprotein E inhibition of vascular smooth muscle cell proliferation but not the inhibition of migration is mediated through activation of inducible nitric oxide synthase. *Arterioscler Thromb Vasc Biol*. 20(4):1020-1026.
31. Moore, Z., B. Zhu, D. Kuhel, and D. Hui. 2004. Vascular apolipoprotein e expression and recruitment from circulation to modulate smooth muscle cell response to endothelial denudation. *Am J Pathol*. 164(6):2109-2116.
32. Campbell, J., M. Reardon, G. Campbell, and P. Nestel. 1985. Metabolism of atherogenic lipoproteins by smooth muscle cells of different phenotype in culture. *Arteriosclerosis*. 5(4):318-328.
33. Sanyour, H., N. Li, A. Rickel, J. Childs, C. Kinser, and Z. Hong. 2019. Membrane cholesterol and substrate stiffness co-ordinate to induce the remodelling of the cytoskeleton and the alteration in the biomechanics of vascular smooth muscle cells. *Cardiovasc Res*. 115(8):1369-1380.
34. Sanyour, H., J. Childs, G. Meininger, and Z. Hong. 2018. Spontaneous oscillation in cell adhesion and stiffness measured using atomic force microscopy. *Sci Rep*. 8(1):2899.
35. Sanyour, H., N. Li, A. Rickel, H. Torres, R. Anderson, M. Miles, J. Childs, K. Francis, J. Tao, and Z. Hong. 2020. Statin mediated cholesterol depletion exerts coordinated effects on the alterations in rat vascular smooth muscle cell biomechanics and migration. *J Physiol*.
36. Amo, C., and R. Garcia. 2016. Fundamental High-Speed Limits in Single-Molecule, Single-Cell, and Nanoscale Force Spectroscopies. *ACS Nano*. 10(7):7117-7124.
37. Butt, H.-J., and M. Jaschke. 1995. Calculation of thermal noise in atomic force microscopy. *Nanotechnology*. 6(1):1-7.
38. Hutter, J. L., and J. Bechhoefer. 1993. Calibration of atomic-force microscope tips. *Review of Scientific Instruments*. 64(7):1868-1873.

566 39. Hong, Z., Z. Sun, M. Li, Z. Li, F. Bunyak, I. Ersoy, J. Trzeciakowski, M. Staiculescu, M. Jin,
567 L. Martinez-Lemus, M. Hill, K. Palaniappan, and G. Meininger. 2014. Vasoactive agonists
568 exert dynamic and coordinated effects on vascular smooth muscle cell elasticity,
569 cytoskeletal remodelling and adhesion. *J Physiol*. 592(6):1249-1266.
570 40. Getz, G., and C. Reardon. 2016. ApoE knockout and knockin mice: the history of their
571 contribution to the understanding of atherogenesis. *J Lipid Res*. 57(5):758-766.
572 41. Khatibzadeh, N., A. Spector, W. Brownell, and B. Anvari. 2013. Effects of plasma
573 membrane cholesterol level and cytoskeleton F-actin on cell protrusion mechanics. *PLoS*
574 *One*. 8(2):e57147.
575 42. Bernecker, C., H. Köfeler, G. Pabst, M. Trötzmüller, D. Kolb, K. Strohmayer, S. Trajanoski,
576 G. Holzapfel, P. Schlenke, and I. Dorn. 2019. Cholesterol Deficiency Causes Impaired
577 Osmotic Stability of Cultured Red Blood Cells. *Front Physiol*. 10:1529.
578 43. Yamaguchi, T., and T. Ishimatu. 2020. Effects of Cholesterol on Membrane Stability of
579 Human Erythrocytes. *Biol Pharm Bull*. 43(10):1604-1608.
580 44. Yamaguchi, T., C. Manaka, A. Ogura, and S. Nagadome. 2021. Importance of Cholesterol
581 Side Chain in the Membrane Stability of Human Erythrocytes. *Biol Pharm Bull*. 44(6):888-
582 893.
583 45. Niggli, V., and J. Rossy. 2008. Ezrin/radixin/moesin: versatile controllers of signaling
584 molecules and of the cortical cytoskeleton. *Int J Biochem Cell Biol*. 40(3):344-349.
585 46. Sun, S., D. Adyshev, S. Dudek, A. Paul, A. McColloch, and M. Cho. 2019. Cholesterol-
586 dependent Modulation of Stem Cell Biomechanics: Application to Adipogenesis. *J Biomech*
587 *Eng*.
588 47. Boudreau, N., and M. Bissell. 1998. Extracellular matrix signaling: integration of form and
589 function in normal and malignant cells. *Curr Opin Cell Biol*. 10(5):640-646.

48. Zhang, X., L. R. Flores, M. C. Keeling, K. Sliogeryte, and N. Gavara. 2020. Ezrin Phosphorylation at T567 Modulates Cell Migration, Mechanical Properties, and Cytoskeletal Organization. *International Journal of Molecular Sciences*. 21(2):435.
49. Blindt, R., A. Bosserhoff, J. Dammers, N. Krott, L. Demircan, R. Hoffmann, P. Hanrath, C. Weber, and F. Vogt. 2004. Downregulation of N-cadherin in the neointima stimulates migration of smooth muscle cells by RhoA deactivation. *Cardiovasc Res*. 62(1):212-222.
50. Nuessle, J., K. Giehl, R. Herzog, S. Stracke, and A. Menke. 2011. TGFβ1 suppresses vascular smooth muscle cell motility by expression of N-cadherin. *Biol Chem*. 392(5):461-474.